PR1 Development on Neutron Imaging Application

Y. Saito

Institute for Integrated Radiation and Nuclear Science, Kyoto University

1. Objectives and Allotted Research Subjects: Neutron imaging provides valuable information which cannot be obtained from an optical or X-ray imaging. The purpose of this project is to develop the imaging method itself and also the experimental environment for expanding the application area of the neutron imaging. The allotted research subjects are as follows:

ARS-1: Measurements of Multiphase Dynamics by Neutron Radiography (Y. Saito *et al.*)
ARS-2: Effect of Water Accumulation in Polymer Electrolyte Fuel Cell and the Cell Performances due to the Difference in the Surface Pressure (H. Asano *et al.*)
ARS-3: Influence of Luminance Scatter in Darkbox for Visualization by using Neutron Raidography (H. Umekawa *et al.*)
ARS-4: Frost Deposition Distribution Estimated by Neutron Imaging and its mechanism (R. Matsumoto *et al.*)
ARS-5: Effect of the moisture content of high-strength concrete on the spalling phenomenon under fire (M. Kanematsu *et al.*)
ARS-6: Effects of the mixer shape in a flow-type supercritical hydrothermal reactor as evaluated by neutron radiography (S. Takami *et al.*)
ARS-7: Neutron Imaging of Plant Roots in Soil Containing Organic Materials (U. Matsushima *et al.*)
ARS-8: Development of a method for quantitative estimation of neutron imaging (M. Kitaguchi *et al.*)
ARS-9: In-situ Lithium diffusion behavior in NASICON-Type Structured Lithium Ion Conductive Composite by Means of Neutron Radiography (S. Takai *et al.*)
ARS-10: Flow Visualization of Liquid Infiltrating into Complex Structures (M. Kaneda *et al.*)

2. Main results and the contents of this report: To develop neutron imaging, our imaging system was developed so that high-speed imaging could be performed at thermal neutron flux of 10^7 n/cm^{2}s. Such improved system was shared with all of the project members and valuable results were obtained as follows:

ARS-1 performed visualization of high temperature boiling two-phase flow by high-speed imaging. Test section is a stainless-steel pipe with an inner diameter of 10mm, which was heated by Joule-heating. The neutron experiments were performed at the B4 port. The imaging system used in this study consists of an op-tical image intensifier, a high-speed camera, and an 85 mm optical lens (F1.2) [1]. The frame rate is 1000 fps, and the exposure time is 0.5 ms. From experimental results, it was found that The electrical field effect of the image intensifier due to the Joule heating and the pipe stretching due to the high-temperature cause the image degradation, and they should be clarified for highly accurate void fraction measurement by high-speed neutron imaging.

ARS-2 applied to neutron imaging to water accumulation in Polymer Electrolyte Fuel Cell (PEFC). A PEFC having a single-serpentine gas channel with a cross-sectional area of 1 × 1 mm^2, an electrode area of 20 mm × 20 mm was used. By varying the surface pressure, the water accumulation was measured in the gas diffusion layers (GDLs). From the experimental results, it is considered that the cell performance decreased due to the increase in the diffusion resistance caused by the water accumulation in the GDL.

ARS-3 investigated the effect of neutron scattering on the accuracy of neutron imaging. By using a phantom and a grid system, the influence of the luminescence in a dark box was roughly estimated.

ARS-4 did not perform experiments due to the difficulties for experimental setup.

ARS-5 applied neutron imaging to analysis of vapor pressure in fire spalling of high-strength concrete. Measuring moisture transfer inside concrete quantitatively, how vapor pressure inside concrete affect spalling was considered.

ARS-6 proposed a mixer for the instantaneous heating of the reactant solution and performed neutron radiography measurements to confirm how supercritical water and room-temperature water mixed in the proposed mixer. From the experimental results, it was found that the proposed mixer was expected to produce metal oxide nanoparticles with smaller sizes and a narrower size distribution.

ARS-7 applied neutron imaging to visualization of plant roots in soil containing organic materials. By using heavy water instead of light water, the plant roots could be clearly visualized by neutron imaging at the E2 port.

ARS-8 was trying to develop a method for quantitative estimation of neutron imaging. For this, transmission images of industrial materials such as screws were acquired at different measurement times. From the measurements, it was found that even short imaging time and/or CT could meet the requirements for some purposes.

ARS-10 performed flow visualization of liquid infiltrating into a complex structures simulating an actual vehicle stator coil. Experiments were performed at the B4 port, by varying the flow rate and the heat applied to the structure. From the experimental results, it was concluded the initial liquid temperature is more crucial for effective coolant spreading and cooling.

PR1-1 Measurements of multiphase flow dynamics using neutron radiography

Y. Saito, D. Ito and N. Odaira

Institute for Integrated Radiation and Nuclear Science, Kyoto University

INTRODUCTION: Neutron radiography (NRG) is very useful for visualizing multiphase flow. The flow structure and dynamics of boiling two-phase flow can be measured. In this work, high-speed neutron imaging was applied to observe the phase change behavior in a heated pipe. The axial change of void fraction distribution at different mass fluxes was evaluated.

VOID FRACTION DISTRIBUTIONS OF BOILING TWO-PHASE FLOW: The boiling two-phase flow in the stainless-steel pipe heated by Joule heating is visualized by high-speed neutron imaging. The schematic diagram of the test section is illustrated in Fig.1. The inner diameter of the stainless steel pipe is 10 mm, and the heated length is 300 mm. The heated length is larger than the visualization area of the neutron imaging, so a manual z-axis stage moves the test section axially. In this experiment, image sequences at five places are acquired and arranged because the height of the image is about 75 mm. The neutron imaging experiments are conducted at the B-4 port in KUR. The imaging system used in this study consists of an optical image intensifier, a high-speed camera, and an 85 mm optical lens (F1.2) [1]. The frame rate is 1000 fps, and the exposure time is 0.5 ms. The empty, water-filled, and two-phase images can estimate the void fraction distribution. The experiments are performed by varying mass flux, heat flux, and water subcooling.

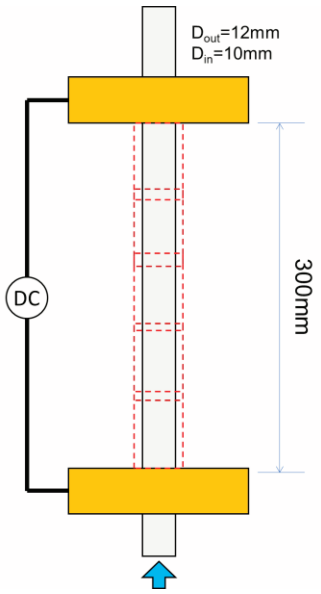

Fig. 1. Schematics of the test section of boiling two-phase flow experiments.

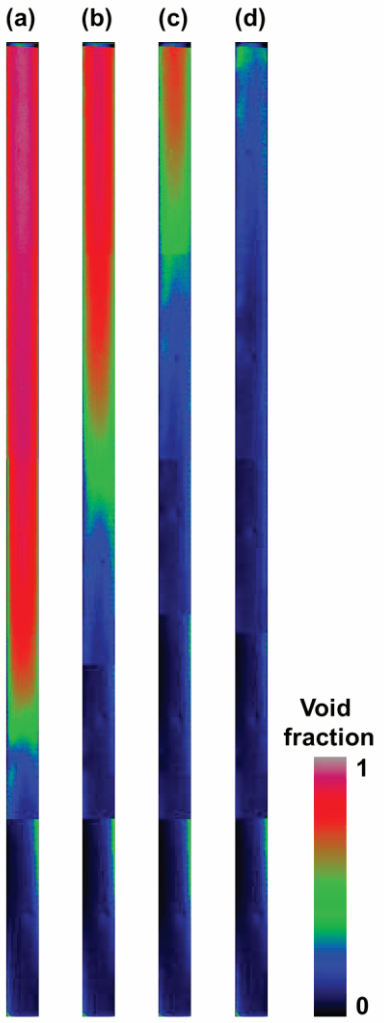

Fig. 2. Void fraction distributions of boiling two-phase flow in a heated pipe; (a) G = 100 kg/m^{2}s, (b) G = 200 kg/m^{2}s, (c) G = 300 kg/m^{2}s, (d) G = 400 kg/m^{2}s.

Fig. 2 shows temporally averaged void fraction distributions estimated from the neutron transmission images. The axial change of the void fraction is investigated by changing the mass flux at q= 290 kW/m^2 and ΔT_{sub}=20K. The boiling two-phase flow structure can be easily understood from these figures. The onset of nucleate boiling moves downstream as the mass flux increases.

The electrical field effect of the image intensifier due to the Joule heating and the pipe stretching due to the high-temperature cause the image degradation, and they should be clarified for highly accurate void fraction measurement by high-speed neutron imaging.

REFERENCES:

[1] D. Ito and Y. Saito, Materials Research Proceedings, **15** (2020) 262-267.

PR1-2 Effect of Water Accumulation in Polymer Electrolyte Fuel Cell and the Cell Performances due to the Difference in the Surface Pressure

H. Murakawa, T. Katanaya, K. Sugimoto, H. Asano, D. Ito[1] and Y. Saito[1]

Graduate School of Engineering, Kobe University
[1]Institute for Integrated Radiation and Nuclear Science, Kyoto University

INTRODUCTION: A polymer electrolyte fuel cell (PEFC) consists of a proton exchange membrane (PEM) sandwiched between gas diffusion layers (GDLs) and gas channels. Water transport in the PEFC is a key topic for fuel cell performance. If water is accumulated in the GDL, it may suppress the air supply to the cathode reaction site. It is well known that the water contents in the PEM are related to the ionic conductivity resulting in a change in the PEFC performances [1]. One of the important parameters for the PEFC setting is the surface pressure, P, of the cell. If the pressure is much higher than the appropriate pressure, the porosity of the GDL may decrease resulting in the decrease of the gas diffusivity. On the other hand, low pressure may lead to an increase in contact resistance. In this study, we focused on the effect of water transport and the cell performances due to the difference in the surface pressure.

EXPERIMENTS: Neutron radiography and electrochemical impedance spectroscopy (EIS) were employed for our investigations. B4-port in Kyoto University Research Reactor was used for the neutron radiography measurements. A PEFC having a single-serpentine gas channel with a cross-sectional area of 1 × 1 mm^2, an electrode area of 20 mm × 20 mm was used. Nafion® membrane and GDLs (SGL 22BB) with a thickness of 200 μm were used. Two-dimensional water distributions were obtained every 60 sec during the PEFC operation for 21 minutes using neutron radiography. The EIS measurement was performed between 20 and 21 minutes after the start of the PEFC power generation for evaluating the PEM resistance and the reaction resistance. The experiments were carried out at room temperature.

RESULTS: Fig. 1 shows an example of the two-dimensional water distribution at a current density, i, of 600 mA/cm^2. The color contour represents the thickness of water along the neutron beam. The gas inlet is placed on the upper right channel. At 5 min, water accumulation is confirmed mainly from between the channels and the ribs. It is considered that the water evacuation from the GDL to the channel easily occurred around the channel corner. At 21 min, much water is confirmed in the gas channel. The water accumulation is greater on the channel than that on the rib position. The average water thickness at the 5th rib which is placed at the center of the serpentine channel was calculated for evaluation of water accumulation in the GDL. Fig. 2 represents the comparison of the time series of the water thickness with different P. The change in the water thickness mainly occurred due to the accumulation in the GDL. For all conditions, the water accumulation occurred significantly during 5 minutes from the power generation start. After that, the change in the water thickness becomes moderate with the operation time. As confirmed by Fig. 1, the change in the water accumulation in the GDL becomes smaller when the water starts to be discharged into the channel. The amount of water accumulation varied depending on the difference in P and the water accumulation was the lowest at P = 1.0 MPa. Table 1 shows the reaction and ohmic resistances at 21 min. The resistances for P = 1.0 MPa take the lowest, indicating the cell performance was the best. Compared with the results in Fig. 2, it can be seen that the cell performance improved due to less water accumulation in the GDL. At P=0.5 and 2.0 MPa, it is considered that the cell performance decreased due to the increase in the diffusion resistance caused by the water accumulation in the GDL.

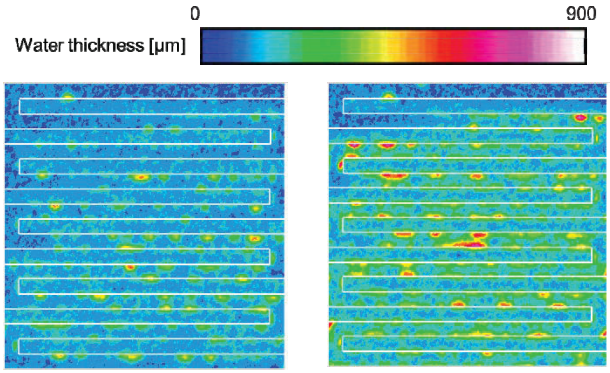

(a) 5min (b) 21 min

Fig. 1. Two-dimensional water distribution at P = 1.0 MPa

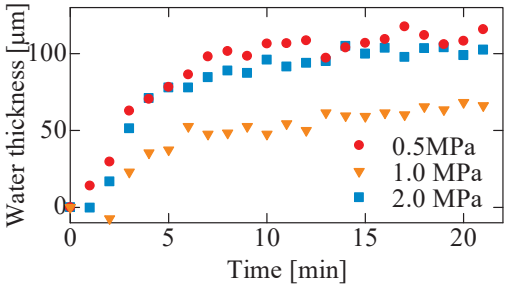

Fig. 2 Time variation of water thickness under the 5th rib.

Table 1. Reaction and ohmic resistances at 21 min.

Surface pressure	Reaction resistance	Ohmic resistance
0.5 MPa	140 mΩ	279 mΩ
1.0 MPa	117 mΩ	117 mΩ
2.0 MPa	131 mΩ	365 mΩ

REFERENCES:

[1] T. E. Springer *et al.*, J. Electrochemical Society, **138** (1991) 2334-2342.

PR1-3 Influence of Luminance Scatter in Darkbox for Visualization by using Neutron Raidography

H. Umekawa[1], Y. Kamiya[1], K. Akiyama[1], T.Ami,
N. Odaira[2], D. Ito[2], Y. Saito[2] and M.Matsubayashi[3]

[1]*Department of Mech. Eng., Kansai University*
[2]*Institute for Integrated Radiation and Nuclear Science, Kyoto University*
[3]*Japan Atomic Energy Agency*

INTRODUCTION: To improve the accuracy of Neutron Radiography, the influence of neutron scatter cannot be neglected. For the calibration of neutron scatter typically three kinds of methods are widely used, as shown in Fig.1. Although these procedures are mainly composed to calibrate the scatter of the neutron, the scatter of luminescence in dark box may also occur. In this report, the influence of the luminescence in a dark box was roughly estimated.

EXPERIMENTAL APPALATUS: For the estimation, the grid system of Fig.2 was used. The Grid and Base Grid , which are made of aluminum, have same configurations. Grids has slits (W:3mm D:6mm), and $Gd(NO_2)_3 \cdot 6H_2O$ is filled and covered by aluminum tape. Base Grid is put above the converter, and Grid set at 100mm distance from the converter. Thus, Base grid absorbs almost of all neutron including the neutron scatter, but the shadow of Grid at 100mm includes the neutron scatter and blur of neutron. Between two Grids, a wedge shape phantom which can be filled by water, is equipped, and transparent length 0mm at the bottom end and 30mm at the top end. Figure 3 is the example of visualization image of these grid system and phantom from the front side.

EXPERIMENTAL RESULTSS: The Gray levels under several experimental conditions at the level of yellow line in Fig.3 are shown in Fig 4. Especially, the difference of gray level between the Base Grid part and the Offset obviously suggests the existence of the scatter of luminescence in the Dark box.

Example of calibration results are shown in Fig.5. In this figure, water thickness of phantom along vertical direction are estimated by using several kinds of Offset values. Especially, to visualize the large attenuation object (thicker part), the influence of luminescence scatter cannot be neglected. This result also suggested that the limitation of the adapting of neutron radiography is approximately 15mm.

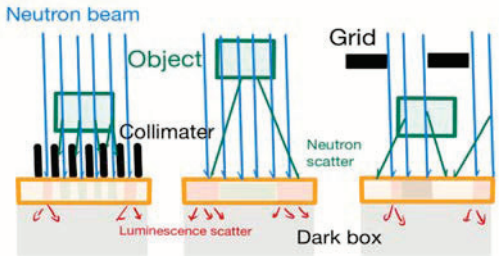

(a) Collimater (b)Gradel (c) Ambra
Fig.1. Calibration methods of Neutron Scatter.

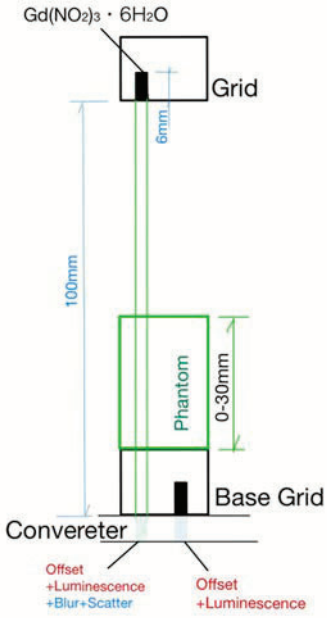

Fig.2. Grid system.

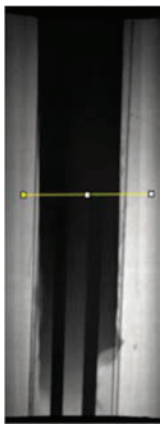

Fig.3. Visualization Image of Phantom and Grid system (Front View) .

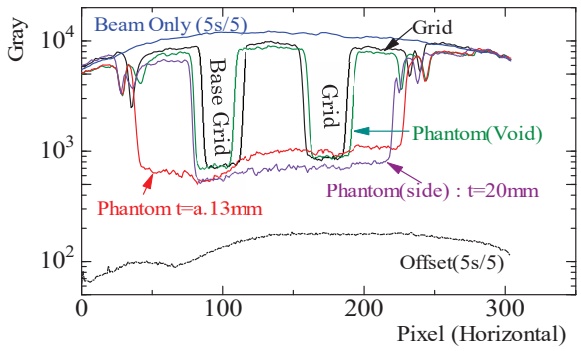

Fig.4. Gray level at the yellow line in Fig.3.

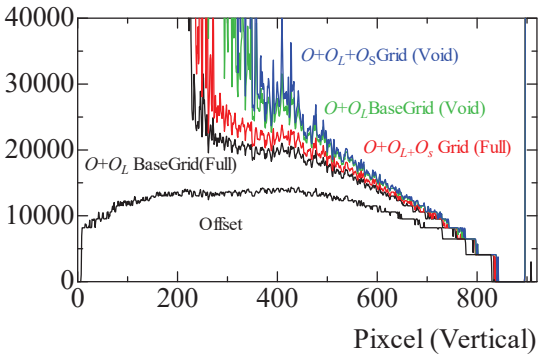

Fig.5. Calibration results. (In this figure, $\log((S_{VOID} - O)/(S - O))$, which is linear to water thickness, is plotted.) .

PR1-4 Effect of the moisture content of high-strength concrete on the spalling phenomenon under fire

M. Yoshioka, T. Hosokawa, E. Noda, M. Kawakami, J. Kim, M. Kanematsu, Y. Nishio[1], N. Odira[2], D. Ito[2] and Y. Saito[2]

Graduate School of Science and Technology, Department of Architecture, Tokyo University of Science
[1]Building Research Institute
[2]Institute for Integrated Radiation and Nuclear Science, Kyoto University

INTRODUCTION: Generally, reinforced concrete buildings are fireproof because they have cover concrete to resist heat from a fire. However, spalling [1] phenomena may occur to lose their cover concrete when the structures were heated by fire, especially when using high strength concrete. In past research, the explanations for this phenomenon have been widely accepted by thermal stress and vapor pressure due to evaporation of internal moisture, or both phenomena. On the other hand, it has been pointed out that the spalling does not occur at the low water content but at the high moisture content. In this study, the effect of moisture content on the spalling phenomena of high-strength concrete was investigated by using the neutron imaging technique.

EXPERIMENTS: Heating experiments were performed on test specimens with target relative moisture contents of 0%, 80%, and 100% in the KUR-B4 port of KURNS. Transmission images were obtained using neutron radiography to detect the moisture behavior inside the concrete. At the same time, temperatures at 10 mm and 20 mm from the heating surface were measured by thermocouples. In addition, the vapor pressure at 10 mm from the heating surface was measured. Stainless steel pipes and silicone oil were used for the measurement to vapor pressure. Fig.1 shows the schematic diagram of the test equipment used in the experiment. The concrete specimens are 100×70×30 mm (width × height × thickness) of reinforcing rebar with a cover depth of 30mm. The compressive strength of concrete measured on the day (25 days after the mixing) of the heating experiments was 135N/mm^2.

RESULTS: Fig.2, shows the distribution of moisture in concrete specimens, a location where the relative moisture content was higher at the time of the explosion than the initial state was confirmed. However, no increase in relative moisture content was observed in the range of 1 mm to 3 mm from the heating surface where the explosion occurred. Therefore, it was not possible to conclude that the movement of water contributed to the occurrence of the explosion inside the concrete. In addition, as shown in Fig.3, the vapor pressure inside the concrete increased as the heating time progressed. This increase was similar to

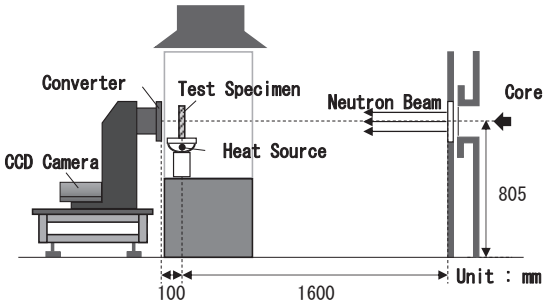

Fig. 1. Schematic diagram of the heating experiment.

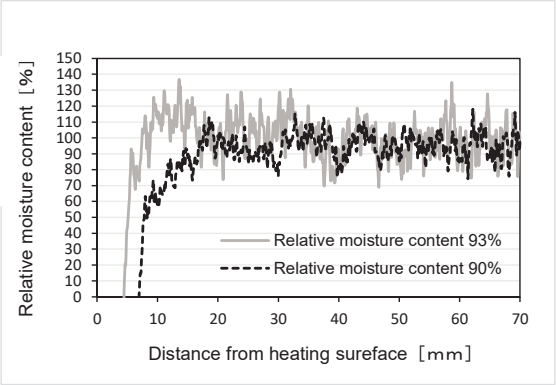

Fig. 2. The effect of initial relative moisture content on the relative moisture distribution just before the spalling.

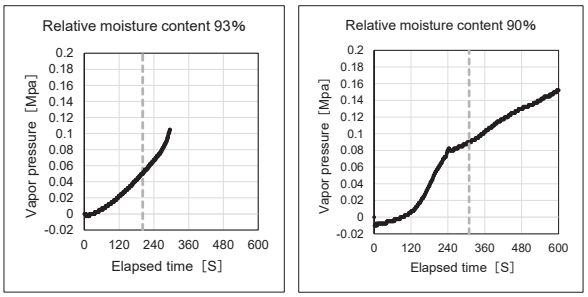

Fig. 3. Temporal changes in vapor pressure inside concrete.

the pressure increase observed in previous studies on test specimens with similar temperature increases. Therefore, it is considered the pressure was measured correctly. Some of the water inside the heated concrete is believed to have produce vapor pressure and exerted force on the concrete. The pressure at the time of the explosion at a position 10 mm from the heating surface was low, ranging from 0.045 MPa to 0.085 MPa, and it is not believed that this value alone caused the explosion. On the other hand, the initial occurrence of the explosion in this experiment was confirmed in the range of 1 mm to 3 mm from the heating surface, so it is possible that the pressure was further increased in this location. In the future, it is necessary to grasp the behavior of moisture at a position closer to the initial location of the explosion and measure the pressure.

REFERENCES:

[1] JCI Committee Report, (2017) JCI-TC-154A.

PR1-5 Effects of the mixer shape in a flow-type supercritical hydrothermal reactor as evaluated by neutron radiography

K. Sato, R. Sasaki, B. Xie, S. Takami, M. Kubo[1], T. Tsukada[2], K. Sugimoto[3], N. Odaira[4], D. Ito[4] and Y. Saito[4]

Graduate School of Engineering, Nagoya University
[1]Graduate School of Engineering, Tohoku University
[2]New Industry Creation Hatchery Center, Tohoku University
[3]Graduate School of Engineering, Kobe University
[4]Institute for Integrated Radiation and Nuclear Science, Kyoto University

INTRODUCTION: Nanoparticle synthesis has attracted considerable attention over the past few decades because nanomaterials exhibit different physical and chemical properties than their corresponding bulk materials. Among various synthesis methods, supercritical hydrothermal synthesis has attracted much attention to synthesize metal oxide nanoparticles. During supercritical hydrothermal synthesis using flow-type reactors, a stream of metal ion aqueous solution was instantaneously heated by mixing with a stream of heated water in a mixer. The previous studies suggested that the reaction rate of metal ions was fast and the products were affected by the course of mixing. In this study, we proposed a mixer for the instantaneous heating of the reactant solution and performed neutron radiography measurements to confirm how supercritical water and room-temperature water mixed in the proposed mixer.[1]

EXPERIMENTS: In this study, we conducted neutron radiography measurements to visualize the mixing behavior in a flow-type reactor. The measurements were performed at the B4 port of the Kyoto University Reactor. The KUR was operated at a 5 MW output with a neutron flux of ca. 5×10^7 n/cm^2 s at the beam exit of the B4 neutron guide tube. The experimental setup (Fig. 1) was similar to that used in previous studies.[2-4] The neutron radiography images were processed to obtain images of the average water density in the mixer. In this study, we used a conventional and designed mixer shape as shown in Fig. 2a and 2d.

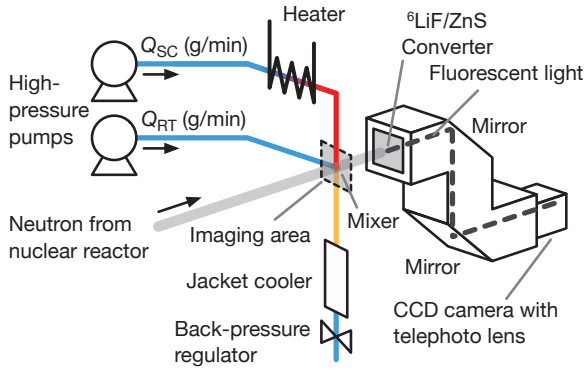

Fig. 1. Diagram of the experimental apparatus.

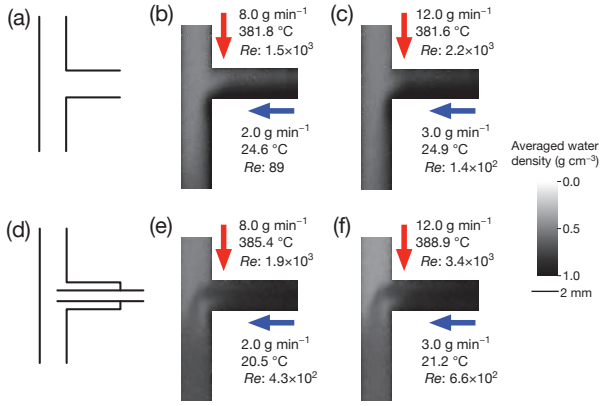

Fig. 2. (a, d) Schematic of conventional (top) and proposed (bottom) mixer and average water density profiles of the (b, c) conventional and (e, f) proposed mixers.

RESULTS: Figs. 2b, 2c, 2e, and 2f show the average water density profiles of both mixers when the flow rates of the supercritical water (Q_{SC}) and room-temperature water (Q_{RT}) were Q_{SC}=8.0 and Q_{RT}=2.0 g/min (Figs. 2b and 2e), and Q_{SC} =12.0 and Q_{RT} =3.0 g/min (Figs. 2c and 2f). The temperatures of the streams are shown in Fig. 2. In Fig. 2, the darker area corresponds to a higher water density, which corresponds to a lower temperature. Figs. 2b and 2c show that room-temperature water supplied from the side flowed along the right wall of the vertical tube after mixing under both flow conditions in the conventional mixer. The supercritical water supplied from the top flowed along the left side of the vertical tube, and the two streams gradually mixed. This mixing behavior resulted in a lower heating rate of the reactant solution, which caused gradual hydrothermal reactions and nanoparticle nucleation. Conversely, this tendency of mixing was apparently different for the proposed mixer shown in Figs. 2e and 2f. The stream of room temperature water flowed out from the side tube with an inner diameter of 1.0 mm and uniformly mixed with the supercritical water supplied from the top. he supplied room-temperature water quickly mixed in the vertical tube after the T-junction. Therefore, the proposed mixer was expected to produce metal oxide nanoparticles with smaller sizes and a narrower size distribution.

REFERENCES:

[1] K. Sato *et al.*, Chem. React. Eng., in press.
[2] S. Takami *et al.*, J. Supercrit. Fluids, **63** (2012) 46-51.
[3] K. Sugioka *et al.*, AIChE J., **60** (2014) 1168-1175.
[4] S. Takami *et al.*, Phys. Proc., **69** (2015) 564-569.

R4P1-6

PR1-6 Neutron Imaging of Plant Roots in Soil Containing Organic Materials

U. Matsushima[1], D. Ito[2], N. Odaira[2], Y. Saito[2]

[1]*Faculty of Agriculture, Iwate University*
[2]*Institute for Integrated Radiation and Nuclear Science, Kyoto University*

INTRODUCTION: Neutron imaging is a technique that takes advantage of the fact that the penetration of neutron beams varies with the material. For example, the thickness of the half-value layer, which is the thickness at which the neutron beam permeability becomes 1/2, is 2 mm and 72 mm for water and silicon, respectively, which are commonly found in soil. This neutron beam can be used to visualize plant roots, which are organic matter containing large amounts of water. When metal-rich soil and water-rich roots were compared in a neutron transmittance image, the image of roots in the soil appeared darker than that of the roots in the soil. However, when organic matter was mixed into the culture medium, the neutron transmittances of the culture medium and roots were similar, making it difficult to distinguish the root image from that of the culture medium. Therefore, roots were visualized in soil containing a high ratio of organic matter using heavy water, which has a lower neutron transmission rate than that of water, as a contrast agent and having the plant roots absorb it.

EXPERIMENTS: Rice husk medium (rice husk:soil = 3:1 by volume) was used as an organic matter-containing medium. The rice husk medium was filled into aluminum containers and Komatsuna (*Brassica rapa* var. *perviridis*) planted into aluminum containers. To allow comparison with neutron images, the thickness of the soil in the direction of neutron irradiation was 2 cm. Neutron images were obtained using the E2 neutron imaging apparatus installed in the research reactor KUR at the Institute for Integrated Radiation and Nuclear Science, Kyoto University. Heavy water was supplied to the roots by immersing them 2 cm deep from the bottom of the sample container in heavy water. Following neutron imaging, the aluminum plates of the growing container were removed and visual images of the roots on the surface of the medium were captured.

RESULTS: First, the distribution of the plant roots within the region of interest (ROI) in the neutron image was estimated by extracting the root region from the optical image of the culture medium surface using binarization (Fig.1-b). In the binary images of the roots, there was no significant difference in the distribution of roots on the surface and underside of the rice husk medium. Therefore, it was analogous that roots in the space inside the medium were also located near the roots that appeared on the surface. In the neutron image of the same ROI, although particles of rice husk medium were observed, the elongated image characteristic of roots was not observed (Fig.1-b). In the rice husk medium supplied with heavy water for waterlogging, only the particle distribution of the medium was observed in the neutron image (Fig.2-a). Therefore, the neutron image at 60 min after the heavy water supply was divided by the image immediately after the heavy water supply to emphasize the change in neutron transmittance. Consequently, an elongated root-like image was observed in the enhanced image (Fig.2-c). This indicated that heavy water was absorbed by the roots from the waterlogged area and replaced the water inside the roots, resulting in lower neutron transmittance in the roots in that area, and the difference appeared as an image. In other words, the use of heavy water as a contrast agent made it possible to visualize the inner roots even in a medium containing a higher ratio of organic matter.

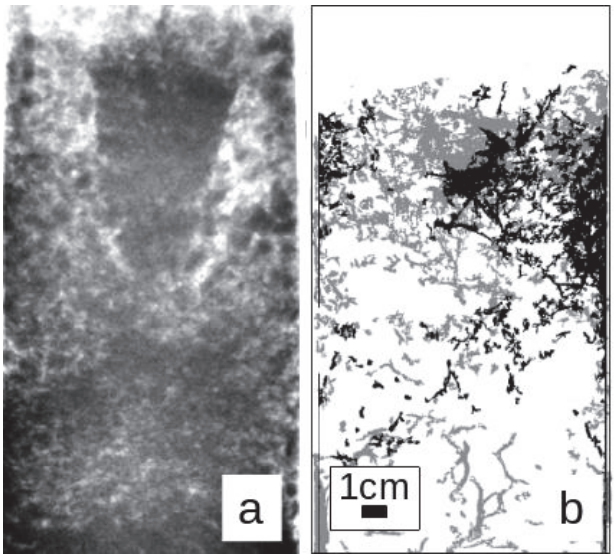

Fig. 1. Neutron image (a) of rice husk medium planted with komatsuna and root zone extracted from an optical image of the same ROI (b). b: Roots on the surface and underside of the sample are shown in black and gray, respectively.

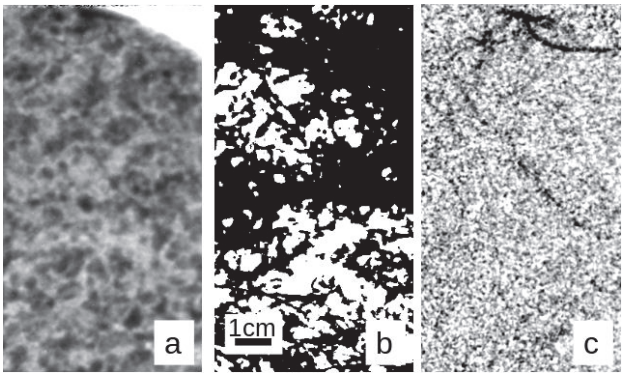

Fig.2. Neutron image (a) of a rice husk medium in which komatsuna was planted, root zone extracted from an optical image of the same ROI (b), and root image contrasted with heavy water (c).

PR1-7 Development of a method for quantitative estimation of neutron imaging

M. Kitaguchi, H. M. Shimizu[1], D. Ito[2], and Y. Saito[2]

KMI, Nagoya University
[1]*Graduate School of Science, Nagoya University*
[2]*Institute for Integrated Radiation and Nuclear Science, Kyoto University*

INTRODUCTION: Neutron imaging and computed tomography (CT) are becoming increasingly important in the development of industrial products. The visualization of microstructures between metals and the distribution of water and organic matter, which cannot be observed with the conventional methods directly, is widely desired. In order to meet the increasing demand, limited beamtime must be allocated and meaningful data must be acquired appropriately. Because neutron imaging differs from visible light and X-rays in many respects in the optical characteristics of the source and device, the experimental setups and measurement times were set empirically. This study aims to establish a technique to quantitatively predict the time required for the measurements. This will enable us to optimize the use of neutrons and to get meaningful conclusions even with small neutron sources with low beam intensity. In addition, the optimal design of new beamline can be performed.

EXPERIMENTS: The measurement was performed at the E2 port where the environment for transmission image measurement was provided. Transmission images of industrial materials such as screws were acquired at different measurement times. In this study, the object was a screw of 2 cm in diameter through a metal part. The contact between the screws and the grease between the parts was the object of interest. The images were taken with the measurement time from 10 seconds to 5 minutes. The internal structure can be seen even with short measurement time.
The CT images were also taken with normal and very-short exposure time. Although the low number of transmitted neutrons make it impossible to analyze the detailed internal structure of a bulk sample, the short-time CT can be used for specific and actual purposes, such as to determine the rough distribution of organic matter inside the sample. We shared the results with the company that provided the test samples and discussed the feasibility of a measurement that would meet their objectives.

DISCUSSION: It was found that even short imaging time and/or CT could meet the requirements for some purposes. It is considered necessary to quantify the requirements.

PR1-8 Observation of Lithium Migration in NASICON-Type Solid Electrolyte by Means of Neutron Radiography

S. Takai[1], H. Takagi[1], T. Yabutsuka[1], T. Yao[2], D. Ito[3], Y. Saito[3]

[1]*Graduate School of Energy Science, Kyoto University*
[2]*Kyoto University*
[3]*Institute for Integrated Radiation and Nuclear Science, Kyoto University*

INTRODUCTION: LISICON-type structured LATP ($Li_{1.3}Al_{0.3}Ti_{1.7}(PO_4)_3$) or LAGP ($Li_{1.5}Al_{0.5}Ge_{1.5}(PO_4)_3$) are promising materials for the solid electrolyte of All-Solid-State Batteries (ASSBs). We have focused on the enhancement of lithium-ion conductivity of these compounds by means of the dielectric particle dispersion technique [1-3]. In recent years, we have successfully measured the tracer diffusion coefficient of lithium ions in LATP by means of neutron radiography emphasizing the contribution of $LaPO_4$ particle dispersion [4]. The isotope of ^{6}Li well attenuates the neutron flux while ^{7}Li does not. We applied ^{6}Li tracer on the LATP block consisting of ^{7}Li and measured the neutron-transmitted images to obtain the diffusion profiles.

While the lithium diffusion was performed simply by annealing in the above study, the lithium-ion migrates between the electrode through the electrolyte in the actual battery operations. Then, we planned to visualize the lithium migration during the solid-state cell operation by constructing test cells. In the previous study, we fabricated the MnO_2 / ^{7}Li-LATP / ^{N}Li-LATP / $Li_{1.33}Ti_{1.67}O_4$ cells to electrolyze for neutron imaging. The natural isotope ratio of ^{6}Li / ^{7}Li is referred to ^{N}Li. However, the lithium transfer at the interface is relatively difficult to observe the lithium migration in ^{7}Li-LATP. In last year, we constructed the $LiMn_2O_4$ / ^{7}Li-LATP / $LiMn_2O_4$ symmetry cell to reduce the solid-solid interface. Nevertheless, the lithium migration across the solid-solid interface is still difficult. In the present study, we employed the LiMn2O4 slurry mixed with acetylene black and PVdF as the electrode materials to keep intimate contact between the electrode and electrolyte.

EXPERIMENTS: ^{7}Li-LAGP ($Li_{1.5}Al_{0.5}Ge_{1.5}(PO_4)_3$) and ^{N}Li-$LiMn_2O_4$ pellets were prepared by the conventional solid-state reaction method. Both sides of the LAGP pellet were polished to achieve the flat plane. $LiMn_2O_4$ powder was mixed with acetylene black and PVdF in the ratio of 8: 1: 1 in weight, which were applied on the both surfaces of the LAGP pellet with a small amount of NMP to fabricate the $LiMn_2O_4$ / ^{7}Li-LAGP / $LiMn_2O_4$ symmetry cells. The typical amount of applied $LiMn_2O_4$ is 3 mg for each side.

The test cell was set in a heater equipment as shown in Fig. 1 and the electric field was applied up to 10 V by using a potentio-galvanostat (Hokuto, HA151). The sample was heated up to 200ºC to facilitate the electrolysis. The subjected current density is selected as 0.2 C.

After the electrolysis was started, the entire apparatus was subjected to a direct neutron beam for 45 minutes at B4 port of KUR (generated at 1MW). Neutron radiography images were taken by the CCD camera (5 min exposure) every 15 minutes. The configuration of the apparatus is also shown in Fig. 1.

RESULTS: The applied voltage gradually increased from 5 V to 10 V, which is the limit for the constant current operation. After reaching the limit potential of 10 V, the electrolysis was continued in constant voltage mode. Fig. 2 represents the typical radiography image after the electrolysis for 60 min. In the present case, any separation of electrode/electrolyte pellets was not observed due to the rigid contact using PVdF. The analysis of transmitted neutrons in the LAGP is presently carried out.

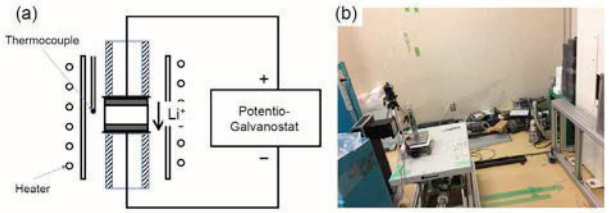

Fig. 1. (a) Schematic diagram of electrolysis equipment and (b) photograph of the experimental configuration.

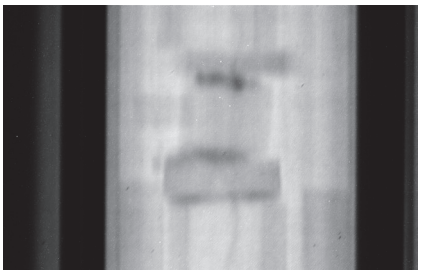

Fig. 2. Typical neutron radiography image of ^{7}Li-LAGP after electrolysis for 60 min.

REFERENCES:

[1] H. Onishi *et al*., Electrochemistry. **84** (2016) 967.
[2] F. Song *et al.,* J. Alloys Compds., **853** (2021) 157089.
[3] F. Song *et al*., *Materials,* **14** (2021) 3502.
[4] F. Song *et al*., *Solid State Ionics,* **377** (2022) 115873.

PR1-9 Flow Visualization of Liquid Infiltrating into Complex Structures

M. Kaneda, Z. Li, and K. Suga

Department of Mechanical Engineering, Osaka Metropolitan University

INTRODUCTION: Electric motors used in electric vehicles have required higher performance, more power, and compactness [1]. This results in higher Joule heating from the motor package and the effective cooling scheme of the heated stator coil has been important. The actual vehicle stator coils are cooled by the coolant poured from a nozzle above. Chen et al. [2] experimented to estimate the removed heat by the coolant from the covered stator coil. In this case, the fundamental characteristic was not clarified in terms of heat and fluid flow. Previously, we experimented with the visualization of the coolant liquid inside the layered structure but it was at room temperature without structure heating. Therefore in this study, the structure was heated by Joule heating and the coolant profile inside the structure was visualized by using neutron radiography.

EXPERIMENTS: The schematic model of the experiment is shown in Fig.1. The coolant liquid was pumped up from the bath and poured onto the horizontal simplified coil structure. The stator coil was presumed by the four-layered accumulated serpentine aluminum plates shown in Fig. 2 which was simplified from the actual stator coil structure where the coolant touches down. The coolant temperature at the nozzle was set at 35 and 50 deg.C to investigate the effect of the initial coolant viscosity. Additionally, the flow rates of the coolant were tested at 500 and 650 mL/min. The applied heat was 100 and 200W. The neutron radiography was conducted inside the structure from the horizontal direction.

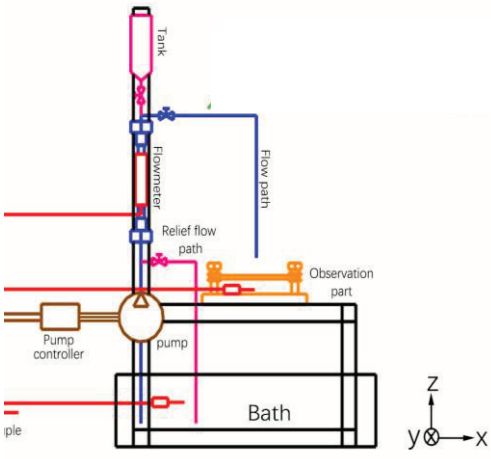

Fig. 1. Experimental setup.

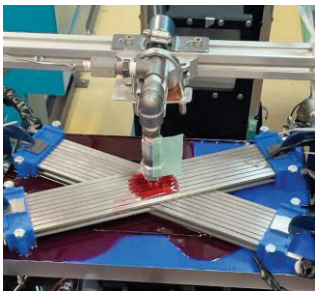

Fig. 2. Simplified heated stator coil.

RESULTS: The visualized coolant profile inside the layer structure is shown in Fig.3. As shown in Figs.3(a) and 3(b), it is found that the coolant profile does not largely depends on the applied heat. This implies the liquid temperature does not increase so much inside the structure so does the liquid viscosity. Indeed, experiments at 50 degC were less affected by the heating amount. Nevertheless, since the heat capacity of the liquid is large enough, sufficient heat removal can be expected. It was confirmed in our laboratory experiment.

Instead of the effect of heating, the liquid profile was largely affected by the coolant temperature at the nozzle (initial temperature) as shown in Fig. 3(c). This is because the liquid viscosity is much smaller at a higher temperature than that at a lower one. Therefore, it can be concluded the initial liquid temperature is more crucial for effective coolant spreading and cooling.

(a) 35 deg C, 100W

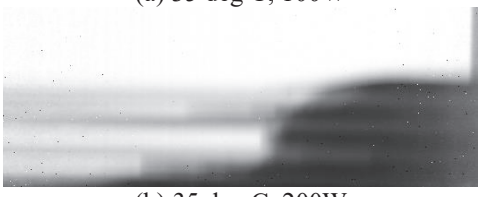

(b) 35 deg C, 200W

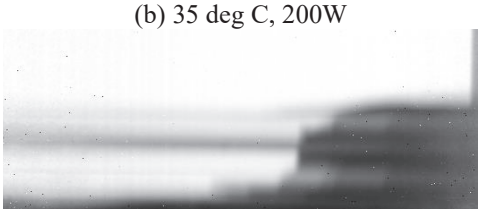

(c) 50 deg C, 100W

Fig. 3. Liquid profile inside the structure at the flow rate of 500 mL/min.

REFERENCES:

[1] N. Kobayashi and T. Ikegami, Thermal Sci. Eng., **15(2)** (2007) 49-54.

[2] P. Chen *et al.,* Appl. Therm. Eng., **220** (2023) 119702.